Journal of Power Sources 309 (2016) 221–230

Contents lists available at ScienceDirect

Journal of Power Sources

journal homepage: www.elsevier.com/locate/jpowsour

Connecting the irreversible capacity loss in Li-ion batteries with the electronic insulating properties of solid electrolyte interphase (SEI) components

Yu-Xiao Lin [a], Zhe Liu [b], Kevin Leung [c], Long-Qing Chen [b], Peng Lu [d], Yue Qi [a, *]

[a] Department of Chemical Engineering and Materials Science, Michigan State University, East Lansing, MI 48824, USA
[b] Department of Materials Science and Engineering, Penn State University, University Park, PA 16802, USA
[c] Sandia National Laboratories, Albuquerque, NM, USA
[d] General Motors Research and Development Center, Warren, MI 48090, USA

HIGHLIGHTS

- A new model to predict electron tunneling barriers and capacity loss was developed.
- The predicted irreversible capacity loss agrees well with experiments.
- 2 nm of LiF or 3 nm of Li_2CO_3 are thick enough to block electron tunneling.
- Electron tunneling barrier decreases under tension and increases under compression.

ARTICLE INFO

Article history:
Received 3 December 2015
Received in revised form
20 January 2016
Accepted 21 January 2016
Available online xxx

Keywords:
Electron tunneling model
Density function theory
Solid electrolyte interphase
Lithium ion battery
Irreversible capacity loss
Stress and strain

ABSTRACT

The formation and continuous growth of a solid electrolyte interphase (SEI) layer are responsible for the irreversible capacity loss of batteries in the initial and subsequent cycles, respectively. In this article, the electron tunneling barriers from Li metal through three insulating SEI components, namely Li_2CO_3, LiF and Li_3PO_4, are computed by density function theory (DFT) approaches. Based on electron tunneling theory, it is estimated that sufficient to block electron tunneling. It is also found that the band gap decreases under tension while the work function remains the same, and thus the tunneling barrier decreases under tension and increases under compression. A new parameter, η, characterizing the average distances between anions, is proposed to unify the variation of band gap with strain under different loading conditions into a single linear function of η. An analytical model based on the tunneling results is developed to connect the irreversible capacity loss, due to the Li ions consumed in forming these SEI component layers on the surface of negative electrodes. The agreement between the model predictions and experimental results suggests that only the initial irreversible capacity loss is due to the self-limiting electron tunneling property of the SEI.

1. Introduction

The grand challenge for rechargeable lithium-ion batteries (LIB) in electric vehicles is to simultaneously improve the battery performance, life, cost, and abuse tolerance [1,2]. In current lithium-ion batteries, the operating voltage of anode is below the reduction voltage of electrolytes, resulting in electrolyte decomposition into a thin layer formed on the electrode surface. This thin layer is believed to be electronically insulating, preventing further electrolyte reduction reactions. However, it is Li-ion (Li^+) conductive. So it is generally referred as solid electrolyte interphase (SEI) [3–5]. The formation and continuous growth of SEI consume active lithium ions, becoming the main cause of the irreversible capacity loss in the initial and following cycles. Generally, a “stable” SEI on a graphite anode surface, mainly formed during the first cycle by consuming about 10%–20% of the initial capacity, should provide the excellent cycling performance of graphite anode materials [6,7]. However, no “stable” SEI has been found to form on high capacity anode materials such as silicon and tin, due to their large volume change during cycling [8–10]. Open questions remain: how does an SEI grow and become stable under certain conditions and how does

* Corresponding author.
E-mail address: yueqi@egr.msu.edu (Y. Qi).

http://dx.doi.org/10.1016/j.jpowsour.2016.01.078
0378-7753/

the SEI contribute to the irreversible capacity loss at the first cycle and the capacity fading in following cycles?

To explain the electronic insulating mechanism of SEI, the concept of electron tunneling model was first put forward by Peled, assuming that an SEI layer on an electrode needs to be thick enough to block electron tunneling [11]. This has been widely accepted but not quantified. In fact, assuming that the height and the shape of the tunneling potential barrier are known, Simmons derived a formula for the current flow through the insulating film sandwiched between two electrodes by the electric tunneling effect in as early as 1963 [12]. Recently, Li *et al.* developed an analytical model based on electron tunneling to predict the relationship between irreversible capacity loss and the cycle number. The tunneling barrier with a square shape was estimated to be in the range of 2.8–2.9 eV [13]. Leung used *ab initio* molecular dynamics (AIMD) and constrained DFT (cDFT) to model the electrolyte decomposition dynamics when a 0.7–1 nm thick artificial oxide SEI layer is coated on a LiC_6 electrode. He estimated the energy barrier and revealed that the thin SEI layers slow down the electron transfer rate because of its electron tunneling barrier [14,15]. However, the size limitation of DFT-based calculations inhibits direct simulation of thicker SEI layers in a full electrode/SEI/electrolyte model. Recently, progresses were made in applying density function theory (DFT) to calculate electronic tunneling in different applications, such as the gold/electrolyte interface [16,17], molecular transistors [18], Schottky barriers formed by metal/CNT [19] and metal/h-BB [20], while challenges still remain in accurately predicting the unoccupied electron states or nonequilibrium tunneling phenomena [21]. Nevertheless, inspired by some success of DFT calculation in predicting tunneling phenomena, we will first compute the electron tunneling barrier in SEI covered anodes using DFT and then develop an electron tunneling model to evaluate the electronic insulating abilities of different SEI components.

The chosen SEI components include inorganic components commonly found in naturally formed SEI, such as LiF and Li_2CO_3; and another excellent solid electrolyte, Li_3PO_4. Based on previous research, it is generally agreed that the SEI on an anode surface can be further divided into to two layers [22–24]. The outside layer interfaced with electrolyte is a porous organic layer. The inside layer in contact with the anode surface is a compact inorganic layer that consists of Li_2CO_3, LiF and Li_2O. The formation of SEI can be considered as two step reduction reactions of solvent molecules (EC and DEC) and lithium salt ($LiPF_6$ or $LiBF_4$). In the first step, the solvents reacted with lithium ions and electrons, and are reduced to organic reduction products, which will form the porous organic layer. In the second step, under the reactions with lithium ions and electrons, the lithium salts together with these organic products are further reduced to inorganic components, such as Li_2CO_3, Li_2O and LiF. According to the reference [25,26], the electrolyte solvents are likely to diffuse through the organic layer along with the observed anion BF_4^-, as they have similar size. Thus, if any electron leaks out of the dense layer, the electrolyte and the anion of the salt trapped in the porous layer can still be further reduced. Therefore, the electronic isolating property of the overall SEI should mainly be provided by the dense inorganic layer.

Lately, there were many efforts to develop coating materials to protect the anode surface as an artificial SEI layer [27,28]. It was anticipated that the coating layer should also block the tunneling of electrons and allow the transfer of lithium ions. Thus, it is important to evaluate the electron tunneling properties of the inorganic components in both naturally formed SEI and artificial SEI candidates. Many of these coatings materials are dense inorganic compounds, such as Al_2O_3, TiO_2 and TiN [27,29]. Among all the coating materials, Li_3PO_4 is an excellent choice due to its chemical stability, insulating property, ionic conductivity and also mechanical property [30–32].

Currently, basic materials properties, such as mechanical, ionic and electronic transport properties of SEI, especially the inorganic component, are not clearly understood mainly due to the thinness of the SEI films, chemical diversity, complex formation mechanism, along with the chemical sensitivity and high cost of *in situ* characterization methods [25,33,34]. Investigations on the material properties of single SEI component either computationally or experimentally have provided important insights for understanding SEI in general. For example, the mechanical properties of bulk LiF and Al_2O_3 have both been measured and computed [35–38]. The lithium ion transport mechanisms in LiF, Li_2CO_3, Li_3PO_4 and NaF were investigated intensively by first principles calculations [26,32,39,40]. However, the electronic insulating mechanism of SEI still remains unknown, and little effort has been made to connect the electron insulating ability of different SEI components to battery capacity loss. In this paper, based on the tunneling barrier obtained from DFT calculations, we developed a simple analytical model to estimate the first cycle irreversible capacity loss and compare its predictions with experimental measurements.

It is well known that the volume expansion upon lithiation in graphite is about 10% [41]. Verbrugge et al. have developed an analytical model for a core-shell structure [42,43], and found the SEI shell will be mechanically stable on graphite but will not tolerate the large deformation of Sn or Si [44,45] due to lithiation. However, it is not clear if the stress in SEI induced by electrode volume expansion [46] will change the electronic tunneling properties of the SEI components. This information is especially important for the understanding on how the repeated volume expansion and contraction gradually cause the increase in reversible capacity loss and electrode degradation in the following cycles [7,47].

This paper is arranged as the following. In section 2, model details how to calculate the electronic tunneling barrier, predict capacity loss due to SEI formation, and investigate the influence of stress were introduced. In section 3.1–3.3, the values of DFT predicted work function and band gap are listed and discussed. In section 3.4, the capacity loss due to SEI thickness and tunneling barrier is predicted and compared with experimental results. In section 3.5, a further investigation on the influence of stress on the predicted electronic tunneling barrier and capacity loss is conducted.

2. Methods

2.1. DFT computed electron tunneling barrier

As SEI is the interphase between anode and electrolyte, if any excess electron from the electronic conducting electrode tunnels through the electronic insulating SEI component to reach electrolyte, it has to overcome the electronic tunneling energy barrier (ΔE_t) from the Fermi level (ε_f) of lithium anode to the bottom of the conduction band of SEI component, as illustrated in Fig. 1. Furthermore, the Fermi level of electrolyte is lower than that of the anode and the SEI [48,49]. If the electron can tunnel through the SEI, it can easily transfer to the lowest unoccupied molecular orbital (LUMO) of the electrolyte, causing reduction reaction of the electrolyte.

This tunneling barrier can be computed via a metal/insulator interface model [50], similar to the Schottky barrier model in metal/semiconductor interfaces [51,52]. It is worth notice that the band bending and the formation of an electrostatic step at the interface can influence the relaxation of the interface structure [49,53] and change the Schottky barrier, work function and electronic structures [54–56]. Special Li/LiF, Li/Li_2CO_3, and Li/Li_3PO_4 interface

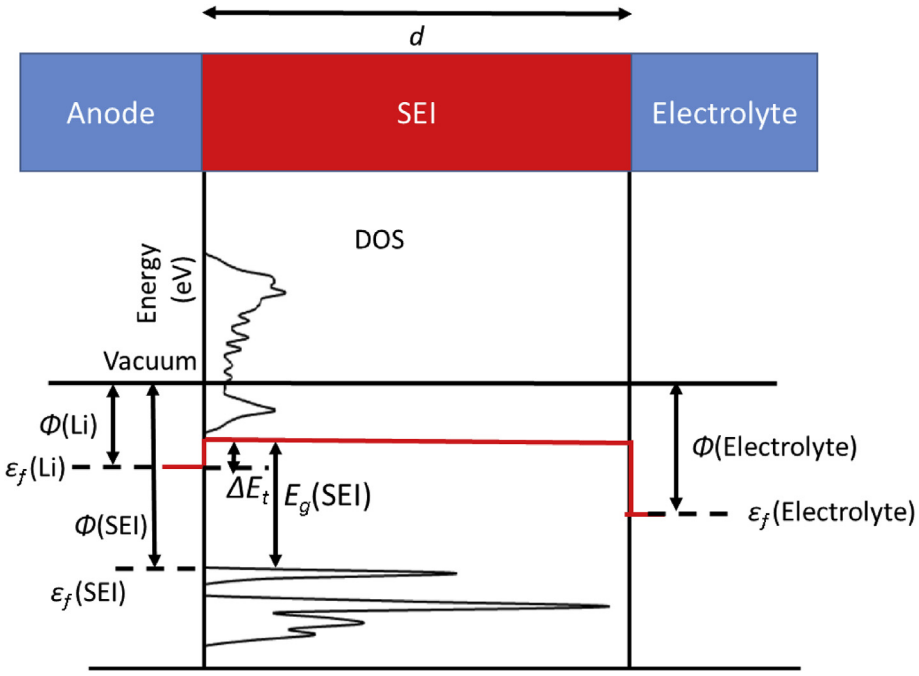

Fig. 1. Calculation of electron tunneling barrier (ΔE_t) by aligning the Fermi level (ε_f), work function (Φ) and band gap (E_g) of the lithium anode and SEI.

structures were constructed and investigated via DFT [30,57]. However, the SEI component layer was limited within 2–3 layers (half of values used in the paper due to symmetry), which sometimes are not thick enough to give converged work functions (as we shall show in section 3.1). Fortunately, the interface region of bend bending is usually less than 5A thick at metal/semiconductor interfaces, and will be even thinner at metal/insulator interfaces. As many experimental evidences suggest that the SEI thickness is beyond nanometers, much thicker than the interface region, the SEI component can be treated as a bulk structure.

Therefore tunneling barriers will be computed based on single components without considering the atomistic details of the interface structures. However, the value of Fermi level obtained by the DFT calculations is one of the Kohn-Sham eigenvalues of the system. Its absolute value does not correspond to the value of Fermi level in the experiment and cannot be compared among different materials. On the other hand, the work function, $\Phi = E_{vac} - \varepsilon_f$, of different materials all share a common reference, vacuum, where the electron potential is zero. Therefore, the Fermi levels of lithium anode and SEI component can be aligned though the comparison of work functions, since they share the same vacuum potential (E_{vac}) as the reference. Aligning the work functions of different materials will permit comparison of their Fermi levels. Furthermore, the electron potential level of the bottom of the conduction band of SEI components is obtained by calculating the density of states (DOS) and the band gap E_g of each SEI component. Thus, the electron tunneling barrier can be obtained by

$$\Delta E_t = E_g(SEI) - \Phi(SEI) + \Phi(Li\_electrode) \quad (1)$$

Fig. 1 illustrated this model of calculating the ΔE_t based on the work function (Φ) and band gap (E_g) of lithium and SEI components, which can all be obtained through DFT calculations.

The lithium anode was chosen as the typical zero voltage reference state in Li-ion batteries. For other anode materials, such as graphite or silicon, the absolute value of electronic tunneling barrier and probability can be obtained by shifting the Fermi level to the corresponding lithiated anodes. For example, the fully lithiated graphite or Si has a voltage of about 0.1V experimentally with respect to Li metal. This voltage is actually the Fermi level of electrons, thus the tunneling barrier, ΔE_t, will increase by about 0.1eV. However, the ΔE_t ordering for the SEI components will remain the same.

All calculations in this study were based upon the implementation of plane wave DFT in the Vienna *ab initio* simulation package (VASP). Potentials constructed with the full potential projector augmented wave (PAW) method were used for the elemental constituents. The exchange-correlation part of the density functional was treated within the generalized gradient approximation (GGA) and Perdew–Burke–Ernzerhof (PBE) functional [58]. As mentioned in section 1, the chosen SEI components include inorganic components commonly found in naturally formed SEI, such as LiF and Li_2CO_3; and a solid electrolyte, Li_3PO_4. Their atomic structures, symmetries, and lattice parameters together with the cutoff energies and **k**-point meshes for bulk calculations are listed in Table 1 [17,39,40]. The level of convergence was set to be 0.001 eV/atom. The bandgaps are computed from these bulk structures. The calculation of work function requires slab models. The surface orientations with the lowest surface energy are chosen in the slab model, and a 10 Å thick vacuum layer is added to prevent interactions between two free surfaces. According to previous research and our test calculations, these orientations are Li_2CO_3 (001), Li_3PO_4 (010) and LiF (100) [17,39,40]. The surfaces are terminated by Li, because it will preserve the stoichiometry of an SEI component and is also reasonable considering the availability of lithium ions. During structure relaxation, ions can be relaxed while the cell volume and cell shape were fixed, and the top and bottom surfaces are symmetrical to each other.

2.2. Predictive capacity loss due to SEI formation and tunneling barrier

The electronic insulating ability of the SEI components can be evaluated by the tunneling probability (T) according to a 1D WKB tunneling theory in quantum mechanics [59],

Table 1
Atomic structures and lattice constants minimized by DFT calculations with the parameter setting for Li_2CO_3, Li_3PO_4 and LiF crystals. The lattice constants shown in parentheses are experimental data [17,39,40]. Li, C, O, P and F atoms at the lattice sites are represented by purple, gray, red, green and blue spheres, respectively.

Component and orientation	Lattice constants (a,b,c, α, β, γ)	Atomic structure	Cut off energy (eV)	K-points grid
Li_2CO_3 Monoclinic C2/C	8.402 Å (8.359 Å), 5.029 Å (4.974 Å), 6.207 Å (6.194 Å), 90°, 114.15° (114.79°), 90°	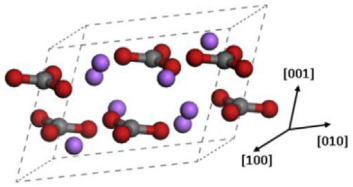	900	4 × 4 × 4
LiF Cubic FM-3M	4.067 Å (4.035 Å), 90°	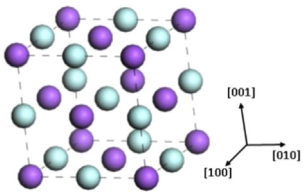	800	4 × 4 × 4
Li_3PO_4 Orthorhombic PNMA	10.554 Å (10.490 Å), 6.155 Å (6.120 Å), 4.978 Å (4.927 Å), 90°	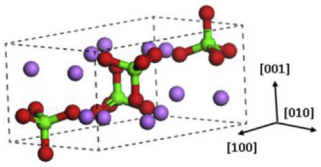	800	6 × 6 × 6

$$T = \frac{16\varepsilon_f \cdot \Delta E_t}{\left(\varepsilon_f + \Delta E_t\right)2} e^{-\frac{4\pi d}{h}} \sqrt{2m \cdot \Delta E_t} \tag{2}$$

where d is the thickness of SEI, m is the mass of electron and h is Planck constant. As we noted in the WKB approximation in quantum tunneling, the obtained tunneling probability in Equation (2) is actually determined by $\Delta E_t d$. Thus, the contribution of electrostatic step at the interface is much less important than that from the bulk region. This further supports our approach of using bulk models.

A simple predictive model can be further developed to estimate how much the irreversible capacity loss, C_{ir}, is in the first few cycles. This is the amount of Li consumed to form the SEI layer that reaches the critical thickness, d^*, to block electron tunneling on the electrode surface. Assuming that complete electron insulating is achieved when $T = e^{-40}$, the critical thickness of SEI, d^* can be obtained from Equation (2).

The number of lithium ions consumed (N) in the SEI component that forms on a unit surface area of anode is

$$N = \rho d^* \tag{3}$$

where ρ is the number of lithium ions per unit volume in SEI component. The irreversible capacity loss is typically defined as the ratio between the lithium ions lost in SEI formation and the cycling lithium ions stored in the host electrode. Thus, the irreversible capacity loss (C_{ir}) due to SEI formation on an anode can be represented as

$$C_{ir} = \frac{M_h A_h \rho d^*}{N_h N_a} \tag{4}$$

where M_h is the molar mass of the host material, N_h is the number of Li ions stored per host atom, A_h is the Brunauer–Emmett–Teller (BET) specific surface area (area/weight) of host material, and N_a is the Avogadro constant. According Equation (4), there is a linear relationship between C_{ir} and A_h. Therefore we define their ratio as the specific area irreversible capacity loss, C, as $C = \frac{C_{ir}}{A_h}$. To facilitate a comparison with the experimentally measured irreversible capacity loss on various types of graphite [60], C for graphite can be represented as $C = \frac{C_{ir}}{A_h} = \frac{6M_h \rho d^*}{N_a}$.

2.3. Loading conditions estimated by stress-strain relationship

In order to investigate how electronic tunneling barrier and probability will change under stress, various states of strain were imposed to LiF. Verbrugge *et al.* developed an analytical model for a core-shell structure and found the hoop stress in the SEI layer may lead to fracture and delamination [58,59]. Thus, we will mainly focus on the normal stress rather than shear stress in the SEI. Various loading conditions can be imposed on a SEI and result in normal strain, according to stress-strain relations for linear elastic solid,

$$\begin{pmatrix} \varepsilon_{11} \\ \varepsilon_{22} \\ \varepsilon_{33} \end{pmatrix} = \frac{1}{E} \begin{pmatrix} 1 & -\nu & -\nu \\ -\nu & 1 & -\nu \\ -\nu & -\nu & 1 \end{pmatrix} \begin{pmatrix} \sigma_{11} \\ \sigma_{22} \\ \sigma_{33} \end{pmatrix} \tag{5}$$

where σ, ε, ν and E are stress, strain, Poisson ratio and Young's modulus, respectively.

LiF was chosen as a representative SEI component for this study because its cubic symmetry allows a unified model to describe the dependence of band gaps on strain. In this study, four different loading conditions were applied on bulk LiF, including hydrostatic stress, uniaxial strain, uniaxial stress and biaxial stress (shown in Fig. 5(a) and Table 3). The lattice of LiF was deformed according to the strain tensors in each loading conditions expressed in terms of dimensionless stress, σ/E, and the Poisson ratio of 0.326 [61].

3. Results and discussions

3.1. DFT computed work function

The surface relaxation, surface energy, work function and band

gap may show oscillation with slab thickness and the surface termination due to quantum size effect, an effect caused by different quantization of states of slab model compared with a semi-infinite sample due to the lowering of dimensionality [62–64]. Therefore, it is important to develop a slab model that mimics the bulk property (*eg.* layer spacing) and leads to the converged properties. The surface energy was computed for layer thickness from 1 to 10. The converged surface energies were determined to be 0.163 J/m^2 for Li_2CO_3(001) with 2 layers; 0.326 J/m^2 for LiF(100) with 2 layers; 0.925 J/m^2 for Li_3PO_4(010) with 3 layers, and 0.458 J/m^2 for Li with 2 layers. The calculated surface energies are consistent with most previous calculations [30,65,66].

The calculation of work function was based on these relaxed slab models, and the computed values as a function of slab thickness were shown in Fig. 3. The work function values of all the four materials oscillate with increasing slab thickness, especially when the thickness is about just 1 or 2 atomic layers. This is due to surface relaxation, especially the large surface relaxation in Li_2CO_3. Fig. 2 shows the relaxed structure of Li_2CO_3 slab with different atomic layers together with some values of A(CO_3-010), which represents the angel between CO_3 plane and Li_2CO_3(010) plane. The layer number is also labeled in Fig. 2, which indicates the position of the layer in the slab model. For example, the layers labeled with 1 indicates the surface layers exposed to vacuum in each slab model. We can see two trends in Fig. 2. The first trend is that the top surface relaxation becomes consistent in thicker slab models. For example, the angle between the CO_3 plane and the surface plane is 0.2° in the monolayer model and 13.3° in the two layer model. But for the slabs thicker than 3 layers, it becomes stable at 14.2°. The second trend is that the center of the slab mimics the bulk crystal structure, where this angle is 18.6°. In the 6 layer thick slab model, the angle changes from 14.2° at the surface layer to 18.4° in the second layer and 19.2° in the third layer. These two trends are also valid for slab models of Li_3PO_4 and LiF, while their fully relaxed surface layers are much less deviated from the bulk structure compared to Li_2CO_3. When the slab thickness is more than 4 atomic layers, the oscillation caused by the quantum size effect becomes relatively small, less than 1%. The value of work function is already well converged when the thickness increased to 4 layers.

Therefore, it is reasonable to choose this converged value as the work function of the bulk crystal. The calculated work function agrees well with other experimental or computational data. The widely measured work function of lithium is about 2.95–3.1 eV, which agrees well with our calculation [65,67]. The work function of Li_3PO_4 calculated by Santosh is also in agreement with our calculation [30].

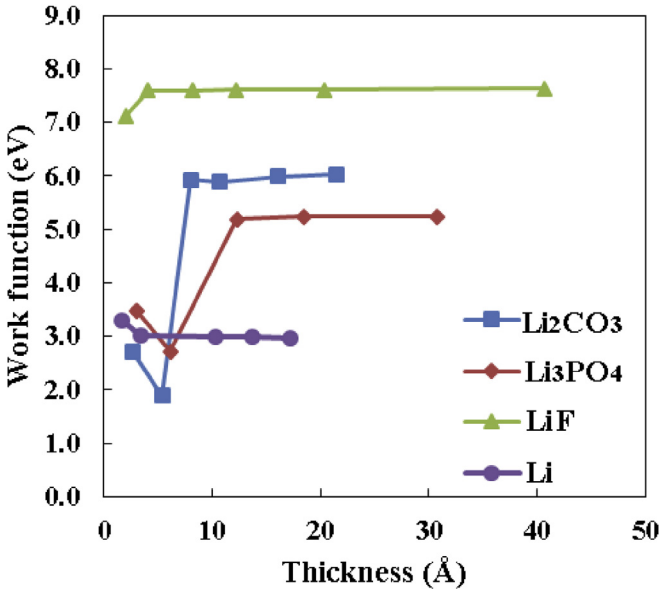

Fig. 3. Work function of Li_2CO_3, Li_3PO_4, LiF and Li as a function of slab thickness.

3.2. Band gap from bulk calculations

The band gap calculation is based on bulk crystal structures, and the results are listed in Table 2. Our calculated band gaps using DFT/GGA are consistent with other computational data using the same method [68–70]. It is well known that calculation by DFT/GGA will underestimate the band gap by up to 50% [71–73]. For example, the band gap of LiF measured in experiment was around 14 eV [74–76],

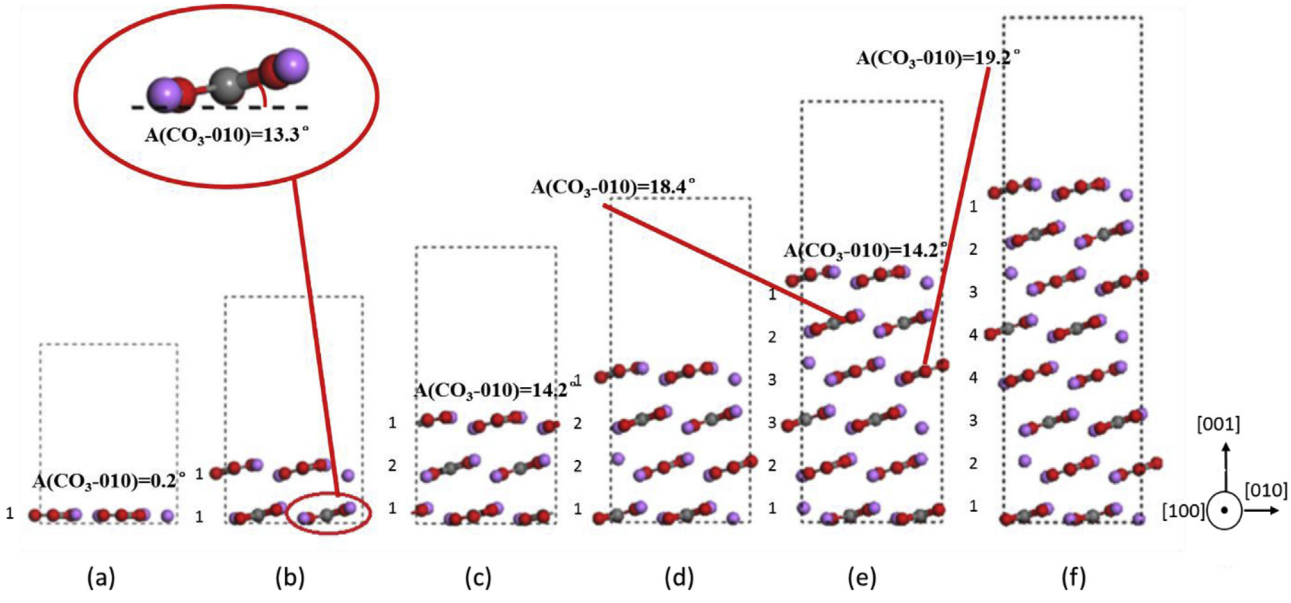

Fig. 2. Relaxed atomic structure of Li_2CO_3(001) slab model with increasing slab thickness.

which is about 80% larger than all the value obtained by DFT/GGA or DFT/LDA. New functions such as Δ(EIG) method [73], hybrid methods [77], GW methods [78] can, in general, improve band gap calculations. We also have applied HSE06 hybrid functions to compute the band gaps for Li_2CO_3, LiF and Li_3PO_4, as listed in Table 2. The bandgap of Li_2CO_3 is 7.07 eV, consistent with a newly reported experiment value of 7.5 eV [79]. The bandgap of LiF and Li_3PO_4 are 10.8 and 8.1 eV, respectively. They are also more consistent with experiment value of 14.1 and 8.0 eV [13,74]. Nevertheless, the consistent underestimation of band gap values from GGA calculations can still provide reasonable estimates of the electronic insulating behavior of the SEI, especially in the comparison of the three insulating SEI components. Due to this underestimation, the tunneling barrier will be underestimated as well. Therefore, we applied a very small tunneling probability e^{-40} as limiting criteria.

We have computed the band gap from the slab model and found the converged band gap is still smaller than that of the bulk crystal. The band gap values also show large oscillation due to quantum size effect when the film thickness is less than 4 atomic layers. A similar trend has been reported by Juaristi, who conducted a DFT calculation on monolayer LiF and obtain a band gap about 6.9 eV, which is also smaller than that of the bulk [80]. The band gap of most semiconductors would increase when the sample size becomes smaller, such as in nano-films, nano-rods or quantum dots [63,64,71], due to quantum confinement effect. This trend is also sensitive to surface termination of a thin film [81]. As it is unclear what will be the surface terminations on the SEI exposed to electrolyte [14], the treatment of SEI as a bulk component when its thickness is larger than 1 nm is still a valid approach. Therefore, we will estimate the tunneling barrier based on the band gap values from bulk crystals.

3.3. Electronic tunneling probability and critical thickness of SEI

As stated in 2.1, the electronic tunneling barrier and probability can be further derived according to Equations (1) and (2). In our model, the electronic tunneling barrier is a constant since both the work function and band gap are converged for the same SEI component. Thus, the electronic tunneling probability is a function that only depends on the thickness of SEI. The critical thickness of SEI, d^*, that blocks electron tunneling can be estimated from Equation (2) assuming a very small tunneling probability $T = e^{-40}$. The d^* values of each SEI component are listed in Table 2, and the order is LiF > Li_3PO_4 > Li_2CO_3 in both GGA and HSE06 methods. The d^* here ranges from 2.0 to 3.0 nm in GGA calculation and 1.6–2.1 in HSE06 calculation, due to the underestimation of band gaps in GGA calculation. Nevertheless, both results are still consistent with both the TEM images by Shim [82] and predicted thickness by Li [13]. In the design of coating layers for anode materials, there are always questions about what the coating materials should be and what thickness is sufficient. Based on the calculation, a ~2 nm LiF can totally block the electronic tunneling. Li_3PO_4 is also an excellent electronic blocking material, and ~2 nm Li_3PO_4 can also block electron tunneling. The thickness of Li_2CO_3 required to block electron tunneling is ~3 nm.

Table 3
Summary of the distance between nearest anions in the original and deformed bulk structure of LiF. k and n represents the ratio between the changed lattice parameter and the original lattice parameter in the direction under stress σ and in the other directions, respectively. r is the distance between nearest anions and η is the normalized average neighbor distance.

	Stress	Strain	η
Hydrostatic Stress	$\begin{pmatrix}1\\1\\1\end{pmatrix}\sigma$	$\begin{pmatrix}1\\1\\1\end{pmatrix}\frac{(1-2\nu)\sigma}{E}=\begin{pmatrix}k-1\\k-1\\k-1\end{pmatrix}$	$\frac{1}{k}$
Uniaxial Strain	$\begin{pmatrix}\frac{\nu}{1-\nu}\\\frac{\nu}{1-\nu}\\1\end{pmatrix}\sigma$	$\begin{pmatrix}0\\0\\\frac{-2\nu^2+1-\nu}{(1-\nu)}\end{pmatrix}\frac{\sigma}{E}=\begin{pmatrix}0\\0\\k-1\end{pmatrix}$	$\frac{1}{3}+\frac{2}{3}*\sqrt{\frac{2}{1+k^2}}$
Uniaxial Stress	$\begin{pmatrix}0\\0\\1\end{pmatrix}\sigma$	$\begin{pmatrix}\nu\\\nu\\1\end{pmatrix}\frac{\sigma}{E}=\begin{pmatrix}1-n\\1-n\\k-1\end{pmatrix}$	$\frac{1}{3n}+\frac{2}{3}*\sqrt{\frac{2}{n^2+k^2}}$
Biaxial Stress	$\begin{pmatrix}1\\1\\0\end{pmatrix}\sigma$	$\begin{pmatrix}1-\nu\\1-\nu\\-2\nu\end{pmatrix}\frac{\sigma}{E}=\begin{pmatrix}k-1\\k-1\\n-1\end{pmatrix}$	$\frac{1}{3k}+\frac{2}{3}*\sqrt{\frac{2}{n^2+k^2}}$

3.4. Estimation of irreversible capacity loss

Based on the d^* values, the number of lithium ions consumed (N) during SEI formation per unit surface area of the anode can be further derived according to Equation (3). Moreover, the irreversible capacity loss (C_{ir}) due to SEI formation can be obtained through Equation (4). The results are also summarized in Table 2. What's more, the irreversible capacity loss scales linearly with the BET surface area of the electrode, at a slope indicated by the specific capacity loss C. The values of C from each SEI component are listed in Table 2. Interestingly, even though the critical thickness of LiF is smaller, the irreversible capacity loss due to LiF formation is larger because the lithium ion density in LiF is almost twice as much as that in Li_2CO_3. It suggests that LiF is a more desirable insulating coating material when the initial capacity loss is not a concern while Li_2CO_3 may be preferred in naturally formed SEI since it causes less capacity loss. This may be difficult to achieve in batteries, since the complicated SEI compositional evolution may be closely related to the kinetics of formation of the different components during SEI formation cycle.

A linear relationship between the first cycle irreversible capacity loss and the BET surface area was reported in Joho's experiments on various carbon electrodes [60]. As shown in Fig. 4, their experimental data suggested a linear relationship between the irreversible capacity loss and BET surface area, and the slope of the linear fitting is $C = 1.18$. Other researches have shown that the active surface area and surface chemistry of anode also play an important role in addition to the total BET surface area in determining the irreversible capacity loss due to exfoliation of graphite during the first cycle [6,83,84]. Thus, the linear fitting of Joho's experimental

Table 2
Calculated results of the tunneling effect in different SEI components. ρ is the number of lithium ions per unit volume in SEI component, Φ, represents the work function, E_g is the band gap (computed from GGA and HSE06), which leads to different electronic tunneling barrier, ΔE_t, the critical thickness of SEI, d^*, and the specific capacity loss, C.

Component	Φ (eV)	ρ (Å^{-3})	Based on GGA				Based on HSE06			
			E_g (eV)	ΔE_t (eV)	d^* (Å)	C (%/(m^2/g))	E_g (eV)	ΔE_t (eV)	d^* (Å)	C (%/(m^2/g))
Li_2CO_3	6.02	0.035	4.75	1.78	30.2	1.27	7.07	4.10	20.0	0.84
LiF	7.59	0.060	8.52	3.98	20.3	1.45	10.8	6.26	16.2	1.15
Li_3PO_4	5.24	0.037	5.68	3.49	21.6	0.96	8.1	5.91	16.6	0.74
Li	3.05	–	0	–	–	–	0	–	–	–

data does not start from the origin and some data points deviate far from the fitting line at small surface area. Considering this part of the irreversible capacity loss, we further draw four lines according to the predicted C values from different SEI components based on both GGA and HSE06 calculation in Fig. 4. The predicted values and the fitting trend line of the experimental data points in Fig. 4 are in good agreement, although the simple model has only assumed one component while the naturally formed SEI is a mixture of Li_2CO_3, LiF, Li_2O and some organic layers. This agreement suggests that the initial SEI thickness and its formation induced initial irreversible capacity loss are likely to be controlled by the self-limiting electron tunneling property of the inorganic components. This also means that the continuous growth of SEI is likely to be caused by other electron transport mechanisms, rather than tunneling.

3.5. Tunneling barrier change due to stress on SEI

LiF was chosen to further investigate the influence of stress on the tunneling barrier. The calculated work function of 10 layers LiF slab model is shown in Fig. 5(b). It can be seen that the change of work function due to stress is quite small. If we just consider the 10% volume change of graphite, the work function can be treated as a constant in this range. However, the band gap values are greatly influenced by deformation. The general trend shown in Fig. 5(b) is that the band gap value (computed with GGA method) increases as the stress changes from tension side to compression side. What is more, under each loading condition, the changes of band gap values are almost linear with respect to the strain (or the ratio between stress and Young's modulus, σ/E), as the trend line in Fig. 5(b) shows.

According to a recent research [85], for ionic crystals where anions are localized, when lattice parameter increases, all bandwidths will shrink and energy states in both valence band and conduction band will increase. However, the shift of more localized valence band will be faster than that of the conduction band. Therefore, the band gap will shrink. This suggests that the distance between anions rather than the distance between anions and cations is the most important parameter, as the electrons are donated to anions. This motivates us to propose a new structure parameter, η, called normalized average anion distance:

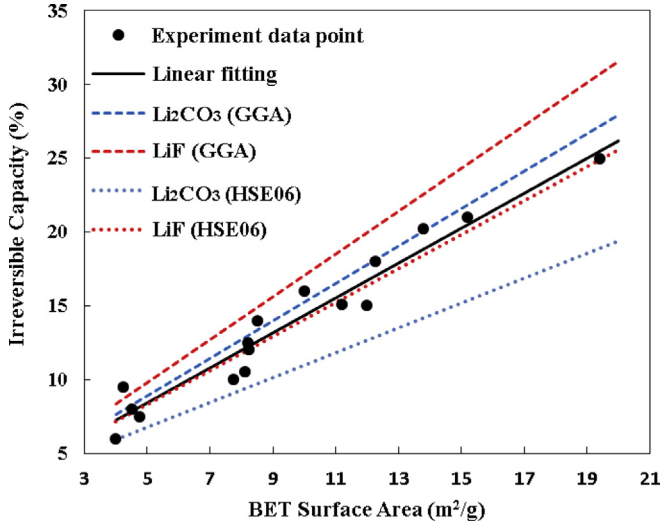

Fig. 4. Predicted initial irreversible capacity loss due to SEI component formation in comparison with experimental data from Joho on various graphite anodes [60].

$$\frac{1}{\eta} = \sum \frac{r_0}{r_i} \tag{6}$$

where r_0 and r are the equilibrium distances between the nearest anions in the perfect structure and deformed structure of LiF, respectively. When calculating the distance between anions, all the 12 nearest anions were included in the sum. η is computed from dimensionless stress (normalized by the Young's modulus) as $\varepsilon=\sigma/E$ for all four loading conditions and is listed in Table 3. For a simpler representation, which demonstrates the connection of η with strain in different direction, k and n were used to represent the ratio between the deformed lattice and the original lattice in specific directions in the strain tensor. The band gap value as a function of η is shown in Fig. 5(c), where η value higher than 1 represents tension while η less than 1 represents compression. Fig. 5(c) clearly shows the band gap value decreases linearly with increasing value of η, and all four loading conditions follow the same function. When the deformation is very large, the band gap values deviate from the linear relationship slightly. In these cases, some 2nd or 3rd nearest neighbor anions become very close to the center anion under large deformation, and should be included in the η calculation. Nevertheless, the normalized anions distance η is a newly proposed parameter to unify the lattice deformation in different loading conditions and the band gap decreases linearly with increasing η. Therefore, the electronic tunneling barrier will decrease under tension and increase under compression.

To further evaluate the effect of the stress on electron tunneling, we estimated the capacity loss of an SEI covered graphite which undergoes 10% volume expansion due to lithiation. First, the SEI formed on graphite is considered stress free. This is reasonable, as suggested by some recent research that the organic part of SEI is formed before lithiation while the inorganic part of SEI is formed simultaneously with lithiation [46,86]. It indicates an SEI film is almost stress-free perpendicular to the particle surface because the organic SEI layer is much softer comparing with the inorganic layer. The inorganic layer of SEI will experience biaxial stress in the other two directions due to the volume expansion of the anode. Due to 10% volume expansion of graphite, the overall thickness of SEI is reduced by 2.1% due to Poisson's ratio. If we only assume that the SEI should grow back to its original thickness in order to block the electrons tunneling, it will lead to 2.1% more irreversible capacity loss. However, the relationship between band gap and η sheds new insight. According to it, the 10% volume expansion of graphite will lead to a 2.0% increase in η. Thus, the band gap will decrease from 8.51 eV to 8.17 eV, leading to 0.34 eV reduction in the tunneling barrier. To achieve the same electronic tunneling probability, the thickness of SEI should increase by another 4.5%, leading to 11.0% more irreversible capacity loss.

4. Conclusions

An electron tunneling model based on density function theory (DFT) calculations was made in order to rank the electronic insulating abilities of different SEI components. The electronic insulating ability can be evaluated by the tunneling barrier, the critical thickness to block electron tunneling (2~3 nm), or Li ions consumed in forming the SEI layer. The initial irreversible capacity loss can be further connected to the DFT calculated tunneling barrier. The agreement between the model and experiment suggests the initial irreversible capacity loss is likely due to the self-limiting electron tunneling property of the SEI. How electronic tunneling barrier and probability change under different types of loading conditions are also investigated. It was shown that the band gap decreases linearly with increasing value of η while the work function stays the same, where η is a new parameter to characterize the average distance

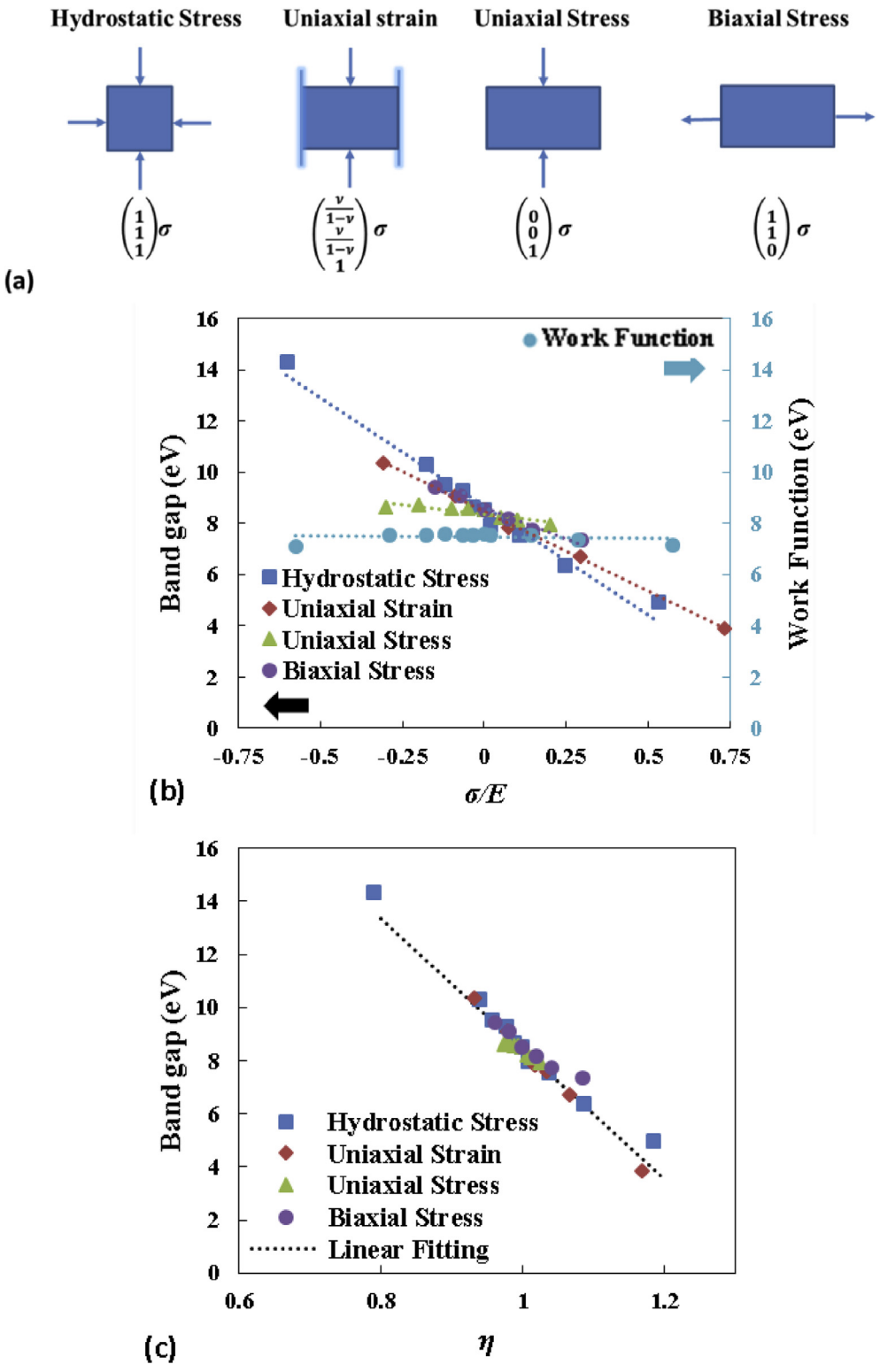

Fig. 5. Schematic of the four loading methods (a), band gap and work function value as a function of σ/E (b) and η (c).

between anions. That means the electron tunneling barrier decreases under tension and increases under compression. To be specific, the 10% volume expansion of graphite will cause about 2.0% decrease in η, making the band gap of LiF reduce from 8.52 eV to 8.17 eV. That means a 4.5% increase in critical thickness of SEI and 11% increase in the irreversible capacity loss considering the deformed structure of LiF.

Although SEI has a mixed structure consisting of both inorganic and organic components, this simple model can still be useful to compare the electronic insulating abilities of different SEI components for SEI design. This simple model also has some limitations. The tunneling barriers estimated from perfect crystals of these SEI

components may also overestimate the tunneling barrier. Other electron transport mechanisms due to defects and polarons need to be considered in order to explain the electron leakage through thicker SEI components (10–100 nm). The simple two layer model that assumes the inorganic layer is dense and the organic layer is permeable for electrolyte may be over simplified. For example, research by Schäfer and Weitzel [87] has shown that ion-doped organic polymer films can fulfill the same job as the inorganic materials, in that case the electron transport may be limited by the doped inorganic material. The two step SEI growth mechanism may also involve other steps, such as porous SEI gradually densifies and dissolution and re-deposition of SEI [88]. Nevertheless, based on current conditions, it is still reasonable to start our investigation from the dense inorganic components, such as LiF, Li_2CO_3, Li_3PO_4.

Acknowledgments

YXL, KL, and YQ acknowledge the support for degradation mechanism modeling as part of Nanostructures for Electrical Energy Storage (NEES), an Energy Frontier Research Center funded by the U.S. Department of Energy, Office of Science, Basic Energy Sciences under Award number DESC0001160. ZL, LQC, PL, and YQ are grateful for the financial support by NSF GOALI under CMMI-1235092. The computer simulations were carried out at MSU High Performance Computer Center (HPCC). Sandia National Laboratories is a multiprogram laboratory managed and operated by Sandia Corporation, a wholly owned subsidiary of Lockheed Martin Corporation, for the U.S. Department of Energy's National Nuclear Security Administration under contract DE-AC04-94AL85000.

References

[1] M. Endo, C. Kim, K. Nishimura, T. Fujino, K. Miyashita, Recent development of carbon materials for Li ion batteries, Carbon 38 (2000) 183–197, http://dx.doi.org/10.1016/S0008-6223(99)00141-4.
[2] M.S. Whittingham, Lithium batteries and cathode materials, Chem. Rev. 104 (2004) 4271–4301, http://dx.doi.org/10.1021/cr020731c.
[3] M. Winter, J.O. Besenhard, M.E. Spahr, P. Novák, Insertion electrode materials for rechargeable lithium batteries, Adv. Mater. 10 (1998) 725–763, http://dx.doi.org/10.1002/(SICI)1521-4095(199807)10:10<725::AID-ADMA725>3.0.CO;2-Z.
[4] P. Verma, P. Maire, P. Novák, A review of the features and analyses of the solid electrolyte interphase in Li-ion batteries, Electrochimica Acta 55 (2010) 6332–6341, http://dx.doi.org/10.1016/j.electacta.2010.05.072.
[5] H. Buqa, A. Würsig, J. Vetter, M.E. Spahr, F. Krumeich, P. Novák, SEI film formation on highly crystalline graphitic materials in lithium-ion batteries, J. Power Sources 153 (2006) 385–390, http://dx.doi.org/10.1016/j.jpowsour.2005.05.036.
[6] S.H. Ng, C. Vix-Guterl, P. Bernardo, N. Tran, J. Ufheil, H. Buqa, et al., Correlations between surface properties of graphite and the first cycle specific charge loss in lithium-ion batteries, Carbon 47 (2009) 705–712, http://dx.doi.org/10.1016/j.carbon.2008.11.008.
[7] M. Wissler, Graphite and carbon powders for electrochemical applications, J. Power Sources 156 (2006) 142–150, http://dx.doi.org/10.1016/j.jpowsour.2006.02.064.
[8] M. Green, E. Fielder, B. Scrosati, M. Wachtler, J.S. Moreno, Structured silicon anodes for lithium battery applications, Electrochem. Solid-State Lett. 6 (2003) A75, http://dx.doi.org/10.1149/1.1563094.
[9] M. Yoshio, S. Kugino, N. Dimov, Electrochemical behaviors of silicon based anode material, J. Power Sources 153 (2006) 375–379, http://dx.doi.org/10.1016/j.jpowsour.2005.05.052.
[10] K. Eom, J. Jung, J.T. Lee, V. Lair, T. Joshi, S.W. Lee, et al., Improved stability of nano-Sn electrode with high-quality nano-SEI formation for lithium ion battery, Nano Energy 12 (2015) 314–321, http://dx.doi.org/10.1016/j.nanoen.2014.12.041.
[11] E. Peled, The electrochemical behavior of alkali and alkaline earth metals in nonaqueous battery systems—the solid electrolyte interphase model, J. Electrochem. Soc. 126 (1979) 2047, http://dx.doi.org/10.1149/1.2128859.
[12] J.G. Simmons, Generalized formula for the electric tunnel effect between similar electrodes separated by a thin insulating film, J. Appl. Phys. 34 (1963) 1793–1803, http://dx.doi.org/10.1063/1.1702682.
[13] D. Li, D. Danilov, Z. Zhang, H. Chen, Y. Yang, P.H.L. Notten, Modeling the SEI-Formation on graphite electrodes in LiFePO4 batteries, J. Electrochem. Soc. 162 (2015) A858–A869, http://dx.doi.org/10.1149/2.0161506jes.
[14] K. Leung, Electronic structure modeling of electrochemical reactions at electrode/electrolyte interfaces in lithium ion batteries, J. Phys. Chem. C 117 (2013) 1539–1547.
[15] K. Leung, Y. Qi, K.R. Zavadil, Y.S. Jung, A.C. Dillon, A.S. Cavanagh, et al., Using atomic layer deposition to hinder solvent decomposition in lithium ion batteries: first principles modeling and experimental studies, J. Am. Chem. Soc. (2011) 14741–14754, http://dx.doi.org/10.1021/ja205119g.
[16] F.C. Simeone, D.M. Kolb, S. Venkatachalam, T. Jacob, The Au(111)/electrolyte interface: a tunnel-spectroscopic and DFT investigation, Angew. Chem. - Int. Ed. 46 (2007) 8903–8906, http://dx.doi.org/10.1002/anie.200702868.
[17] F.C. Simeone, D.M. Kolb, S. Venkatachalam, T. Jacob, Tunneling behavior of electrified interfaces, Surf. Sci. 602 (2008) 1401–1407, http://dx.doi.org/10.1016/j.susc.2008.01.034.
[18] M. Kondratenko, S.R. Stoyanov, S. Gusarov, A. Kovalenko, R.L. McCreery, Theoretical Modeling of Tunneling Barriers in Carbon-Based Molecular Electronic Junctions, J. Phys. Chem. C 119 (2015) 11286–11295, http://dx.doi.org/10.1021/jp5128332.
[19] N. Park, S. Hong, Electronic structure calculations of metal-nanotube contacts with or without oxygen adsorption, Phys. Rev. B - Condens. Matter Mater. Phys. 72 (2005) 1–5, http://dx.doi.org/10.1103/PhysRevB.72.045408.
[20] M. Bokdam, G. Brocks, M.I. Katsnelson, P.J. Kelly, Schottky barriers at hexagonal boron nitride/metal interfaces: A first-principles study, Phys. Rev. B 90 (2014) 085415, http://dx.doi.org/10.1103/PhysRevB.90.085415.
[21] P. Hyldgaard, Density-functional theory of nonequilibrium tunneling, Phys. Rev. B - Condens. Matter Mater. Phys. 78 (2008) 165109, http://dx.doi.org/10.1103/PhysRevB.78.165109.
[22] S. Zhang, M.S. Ding, K. Xu, J. Allen, T.R. Jow, Understanding Solid Electrolyte Interface Film Formation on Graphite Electrodes, Electrochem. Solid-State Lett. 4 (2001) A206, http://dx.doi.org/10.1149/1.1414946.
[23] J. Christensen, J. Newman, A mathematical model for the lithium-ion negative electrode solid electrolyte interphase, J. Electrochem. Soc. 151 (2004) A1977, http://dx.doi.org/10.1149/1.1804812.
[24] I. Shkrob, Y. Zhu, T.W. Marin, D. Abraham, Reduction of carbonate electrolytes and the formation of solid-electrolyte interface (SEI) in lithium-ion batteries. 1. Spectroscopic observations of radical intermediates generated in one-electron reduction of carbonates, J. Phys. Chem. C 117 (2013) 19255–19269, http://dx.doi.org/10.1021/jp406274e.
[25] P. Lu, S.J. Harris, Lithium transport within the solid electrolyte interphase, Electrochem. Commun. 13 (2011) 1035–1037, http://dx.doi.org/10.1016/j.elecom.2011.06.026.
[26] S. Shi, P. Lu, Z. Liu, Y. Qi, L.G. Hector, H. Li, et al., Direct calculation of Li-ion transport in the solid electrolyte interphase, J. Am. Chem. Soc. 134 (2012) 15476–15487, http://dx.doi.org/10.1021/ja305366r.
[27] J. Li, X. Xiao, Y. Cheng, M.W. Verbrugge, Atomic layered coating enabling ultrafast surface kinetics at silicon, J. Chem. Lett. 4 (2013) 3387–3391.
[28] Y. Liu, Z.Y. Wen, X.Y. Wang, X.L. Yang, A. Hirano, N. Imanishi, et al., Improvement of cycling stability of Si anode by mechanochemical reduction and carbon coating, J. Power Sources 189 (2009) 480–484, http://dx.doi.org/10.1016/j.jpowsour.2008.12.045.
[29] E.M. Lotfabad, P. Kalisvaart, A. Kohandehghan, K. Cui, M. Kupsta, B. Farbod, et al., Si nanotubes ALD coated with TiO2, TiN or Al2O3 as high performance lithium ion battery anodes, J. Mater. Chem. A 2 (2014) 2504, http://dx.doi.org/10.1039/c3ta14302c.
[30] K. Santosh, R.C. Longo, K. Xiong, K. Cho, Electrode-electrolyte interface for solid state Li-Ion Batteries: point defects and mechanical strain, J. Electrochem. Soc. 161 (2014) F3104–F3110, http://dx.doi.org/10.1149/2.0151411jes.
[31] N.D. Lepley, N.A.W. Holzwarth, Y.A. Du, Structures, Li+ mobilities, and interfacial properties of solid electrolytes Li_3PS_4 and Li_3PO_4 from first principles, Phys. Rev. B 88 (2013) 104103, http://dx.doi.org/10.1103/PhysRevB.88.104103.
[32] Y.A. Du, N.A.W. Holzwarth, Mechanisms of Li+ diffusion in crystalline γ- and β-Li_3PO_4 electrolytes from first principles, Phys. Rev. B - Condens. Matter Mater. Phys. 76 (2007) 174302, http://dx.doi.org/10.1103/PhysRevB.76.174302.
[33] J. Zheng, H. Zheng, R. Wang, L. Ben, W. Lu, L. Chen, et al., 3D visualization of inhomogeneous multi-layered structure and Young's modulus of the solid electrolyte interphase (SEI) on silicon anodes for lithium ion batteries, Phys. Chem. Chem. Phys. 16 (2014) 13229, http://dx.doi.org/10.1039/c4cp01968g.
[34] N. Weadock, N. Varongchayakul, J. Wan, S. Lee, J. Seog, L. Hu, Determination of mechanical properties of the SEI in sodium ion batteries via colloidal probe microscopy, Nano Energy 2 (2013) 713–719, http://dx.doi.org/10.1016/j.nanoen.2013.08.005.
[35] P.K. Jha, B.N. Jha, Mechanical properties of LiF and LiCl Crystals under high pressure, Phys. Stat. Sol.B 175 (1993) K1.
[36] S.V. Lubenets, E.I. Ostapchuk, L.M. Soifer, F. Appel, H.-J. Kaufmann, The influence of OH−-ions on the mechanical properties in LiF and NaCl single crystals, Cryst. Res. Technol. 19 (1984) 349–356, http://dx.doi.org/10.1002/crat.2170190311.
[37] S.-Y. Kim, Y. Qi, Property evolution of Al_2O_3 coated and uncoated si electrodes: a first principles investigation, J. Electrochem. Soc. 161 (2014) F3137–F3143, http://dx.doi.org/10.1149/2.0301414jes.
[38] E. Söderlund, I. Reineck, D.J. Rowcliffe, Ultralow load indentation hardness and modulus of K − and α−Al2O3 CVD coatings, J. Mater. Res. 9 (1994) 1683–1692, http://dx.doi.org/10.1557/JMR.1994.1683.
[39] S. Shi, Y. Qi, H. Li, L.G. Hector, Defect thermodynamics and diffusion mechanisms in Li_2CO_3 and implications for the solid electrolyte interphase in Li-Ion batteries, J. Phys. Chem. 117 (2013) 8579–8593.
[40] J. Pan, Y. Cheng, Y. Qi, General method to predict voltage-dependent ionic

conduction in a solid electrolyte coating on electrodes, Phys. Rev. B (2015) 1–9, http://dx.doi.org/10.1103/PhysRevB.91.134116, 134116.
[41] B.A. Boukamp, G.C. Lesh, R.A. Huggins, All-solid lithium electrodes with mixed-conductor matrix, J. Electrochem. Soc. 128 (1981) 725, http://dx.doi.org/10.1149/1.2127495.
[42] R. Deshpande, M. Verbrugge, Y.-T. Cheng, J. Wang, P. Liu, Battery Cycle Life Prediction with Coupled Chemical Degradation and Fatigue Mechanics, J. Electrochem. Soc. 159 (2012) A1730–A1738, http://dx.doi.org/10.1149/2.049210jes.
[43] M.W. Verbrugge, Y.-T. Cheng, Stress and strain-energy distributions within diffusion-controlled insertion-electrode particles subjected to periodic potential excitations, J. Electrochem. Soc. 156 (2009) A927, http://dx.doi.org/10.1149/1.3205485.
[44] H. Wu, G. Chan, J.W. Choi, I. Ryu, Y. Yao, M.T. McDowell, et al., Stable cycling of double-walled silicon nanotube battery anodes through solid–electrolyte interphase control, Nat. Nanotechnol. 7 (2012) 310–315, http://dx.doi.org/10.1038/nnano.2012.35.
[45] C.-F. Sun, K. Karki, Z. Jia, H. Liao, Y. Zhang, T. Li, et al., A beaded-string silicon anode, ACS Nano 7 (2013) 2717–2724, http://dx.doi.org/10.1021/nn4001512.
[46] A. Tokranov, B.W. Sheldon, P. Lu, X. Xiao, A. Mukhopadhyay, The origin of stress in the solid electrolyte interphase on carbon electrodes for Li Ion batteries, J. Electrochem. Soc. 161 (2014) A58–A65, http://dx.doi.org/10.1149/2.009401jes.
[47] D. Aurbach, M.D. Levi, E. Levi, A. Schechter, Failure and stabilization mechanisms of graphite electrodes, J. Phys. Chem. B 101 (1997) 2195–2206, http://dx.doi.org/10.1021/jp962815t.
[48] H. Gerischer, Fermi levels in electrolytes and the absolute scale of redox potentials, Appl. Phys. Lett. 43 (1983) 393, http://dx.doi.org/10.1063/1.94356.
[49] A.J. Bard, A.B. Bocarsly, F.R.F. Fan, E.G. Walton, M.S. Wrighton, The concept of Fermi level pinning at semiconductor/liquid junctions. Consequences for energy conversion efficiency and selection of useful solution redox couples in solar devices, J. Am. Chem. Soc. 102 (1980) 3671–3677, http://dx.doi.org/10.1021/ja00531a001.
[50] G. Bordier, C. Noguera, Electronic structure of a metal-insulator interface: Towards a theory of nonreactive adhesion, Phys. Rev. B 44 (1991) 6361–6371, http://dx.doi.org/10.1103/PhysRevB.44.6361.
[51] X.-C. Pan, X. Chen, H. Liu, Y. Feng, Z. Wei, Y. Zhou, et al., Pressure-driven dome-shaped superconductivity and electronic structural evolution in tungsten ditelluride, Nat. Commun. 6 (2015) 7805, http://dx.doi.org/10.1038/ncomms8805.
[52] L. Brillson, The structure and properties of metal-semiconductor interfaces, Surf. Sci. Rep. 2 (1982) 123–326, http://dx.doi.org/10.1016/0167-5729(82)90001-2.
[53] R. Tung, Formation of an electric dipole at metal-semiconductor interfaces, Phys. Rev. B 64 (2001) 1–15, http://dx.doi.org/10.1103/PhysRevB.64.205310.
[54] M. Bokdam, G. Brocks, M.I. Katsnelson, P.J. Kelly, Schottky barriers at hexagonal boron nitride/metal interfaces: a first-principles study, Phys. Rev. B 90 (2014) 085415, http://dx.doi.org/10.1103/PhysRevB.90.085415.
[55] F. Cerbu, H.-S. Chou, I.P. Radu, K. Martens, A.P. Peter, V.V. Afanas'ev, et al., Band alignment and effective work function of atomic-layer deposited VO_2 and V_2O_5 films on SiO_2 and Al_2O, Phys. Status Solidi C. 12 (2015) 238–241, http://dx.doi.org/10.1002/pssc.201400037.
[56] S. Ling, M.B. Watkins, A.L. Shluger, Effects of atomic scale roughness at metal/insulator interfaces on metal work function, Phys. Chem. Chem. Phys. 15 (2013) 19615–19624, http://dx.doi.org/10.1039/c3cp53590h.
[57] Z. Liu, Y. Qi, Y.X. Lin, L. Chen, P. Lu, L.Q. Chen, Interfacial Study on Solid Electrolyte Interphase at Li metal Anode : Implication for Li Dendrite Growth, Journal of Electrochemistry Society 163 (2016) 592–598, http://dx.doi.org/10.1149/2.0151605jes.
[58] J.P. Perdew, K. Burke, M. Ernzerhof, Generalized Gradient Approximation Made Simple, Phys. Rev. Lett. 77 (1996) 3865–3868, http://dx.doi.org/10.1103/PhysRevLett.77.3865.
[59] M. Razavy, Quantum Theory of Tunneling. Singapore, SGP: World Scientific Publishing Co., 2003. ProQuest ebrary. Web. 3 November 2015. Copyright © 2003. World Scientific Publishing Co.. All rights reserved., n.d.
[60] F. Joho, B. Rykart, A. Blome, P. Novák, H. Wilhelm, M.E. Spahr, Relation between surface properties, pore structure and first-cycle charge loss of graphite as negative electrode in lithium-ion batteries, J. Power Sources 97–98 (2001) 78–82, http://dx.doi.org/10.1016/S0378-7753(01)00595-X.
[61] lithium-fluoride-lif-data-sheet.pdf, (n.d.). www.crystran.co.uk/userfiles/files/lithium-fluoride-lif-data-sheet.pdf.
[62] A. Kiejna, J. Peisert, P. Scharoch, Quantum-size effect in thin Al (110) slabs, Surf. Sci. 432 (1999) 54–60, http://dx.doi.org/10.1016/S0039-6028(99)00510-5.
[63] S. Baskoutas, A.F. Terzis, Size-dependent band gap of colloidal quantum dots, J. Appl. Phys. 99 (2006) 013708, http://dx.doi.org/10.1063/1.2158502.
[64] L. Lin, Z. Li, J. Feng, Z. Zhang, Indirect to direct band gap transition in ultra-thin silicon films, Phys. Chem. Chem. Phys. PCCP 15 (2013) 6063–6067, http://dx.doi.org/10.1039/c3cp50429h.
[65] P.T. Salo, R. Laihia, K. Mansikka, First-principles calculations for work function and surface energy of thin lithium films, Surf. Sci. 348 (1996) 168–174.
[66] S.J. Binnie, Ab Initio Surface Energetics: beyond Chemical Accuracy, University College London, 2011. http://discovery.ucl.ac.uk/1318067/.
[67] M. Stossel, J. Staudigel, F. Steuber, J. Simmerer, A. Winnacker, Impact of the cathode metal work function on the performance of vacuum-deposited organic light emitting devices, Appl. Phys. A - Mater 68 (1999) 387–390, http://dx.doi.org/10.1007/s003399900011.
[68] J.E. Saal, S. Kirklin, M. Aykol, B. Meredig, C. Wolverton, Materials design and discovery with high-throughput density functional theory: the open quantum materials database (OQMD), Jom 65 (2013) 1501–1509, http://dx.doi.org/10.1007/s11837-013-0755-4.
[69] Y.-N. Xu, Comparative studies of the electronic structure of $LiFePO_4$, $FePO_4$, Li_3PO_4, $LiMnPO_4$, $LiCoPO_4$, and $LiNiPO_4$, J. Appl. Phys. 95 (2004) 6583, http://dx.doi.org/10.1063/1.1667422.
[70] A. Zunger, A.J. Freeman, Ground- and excited-state properties of LiF in the local-density formalism, Phys. Rev. B 16 (1977) 2901–2926, http://dx.doi.org/10.1103/PhysRevB.16.2901.
[71] B. Delley, E.F. Steigmeier, Size dependence of band gaps in silicon nanostructures, Appl. Phys. Lett. 67 (1995) 2370, http://dx.doi.org/10.1063/1.114348.
[72] S.Q. Wu, Z.F. Hou, Z.Z. Zhu, First-principles study on the structural, elastic, and electronic properties of γ-$LiAlO_2$, Comput. Mater. Sci. 46 (2009) 221–224, http://dx.doi.org/10.1016/j.commatsci.2009.02.028.
[73] P. Scharoch, M. Winiarski, An efficient method of DFT/LDA band-gap correction, Comput. Phys. Commun. 184 (2013) 2680–2683, http://dx.doi.org/10.1016/j.cpc.2013.07.008.
[74] R.C. Chaney, E.E. Lafon, C.C. Lin, Energy band structure of lithium fluoride crystals by the method of tight binding, Phys. Rev. B 4 (1971) 2734, http://dx.doi.org/10.1103/PhysRevB.4.2734.
[75] M. Piacentini, D.W. Lynch, C.G. Olson, Thermoreflectance of LiF between 12 and 30 eV, Phys. Rev. B 13 (1976) 5530–5543, http://dx.doi.org/10.1103/PhysRevB.13.5530.
[76] D. Roessler, W. Walker, Optical constants of magnesium oxide and lithium fluoride in the far ultraviolet, J. Phys. Chem. Solids 28 (1967) 1507–1509, http://dx.doi.org/10.1364/JOSA.57.000835.
[77] M.G. Silveirinha, C.A. Fernandes, A hybrid method for the efficient calculation of the band structure of 3-D metallic crystals, IEEE Trans. Microw. Theory Tech. 52 (2004) 889–902, http://dx.doi.org/10.1109/TMTT.2004.823563.
[78] F. Tran, P. Blaha, Accurate band gaps of semiconductors and insulators with a semilocal exchange-correlation potential, Phys. Rev. Lett. 102 (2009) 5–8, http://dx.doi.org/10.1103/PhysRevLett.102.226401.
[79] M. Vos, G.G. Marmitt, Y. Finkelstein, R. Moreh, Determining the band gap and mean kinetic energy of atoms from reflection electron energy loss spectra, J. Chem. Phys. 143 (2015) 104203, http://dx.doi.org/10.1063/1.4929911.
[80] J.I. Juaristi, On the metallization of the LiF monolayer, Solid State commun. 91 (1994) 957–960, http://dx.doi.org/10.1007/s13398-014-0173-7.2.
[81] R.I. Eglitis, E. Heifets, E.A. Kotomin, J. Maier, G. Borstel, First-principles calculations of perovskite thin films, Mater. Sci. Semicond. Process. 5 (2002) 129–134, http://dx.doi.org/10.1016/S1369-8001(02)00093-8.
[82] J. Shim, R. Kostecki, T. Richardson, X. Song, K.A. Striebel, Electrochemical analysis for cycle performance and capacity fading of a lithium-ion battery cycled at elevated temperature, J. Power Sources 112 (2002) 222–230, http://dx.doi.org/10.1016/S0378-7753(02)00363-4.
[83] P. Novák, J. Ufheil, H. Buqa, F. Krumeich, M.E. Spahr, D. Goers, et al., The importance of the active surface area of graphite materials in the first lithium intercalation, J. Power Sources 174 (2007) 1082–1085, http://dx.doi.org/10.1016/j.jpowsour.2007.06.036.
[84] D. Aurbach, B. Markovsky, I. Weissman, E. Levi, Y. Ein-Eli, On the correlation between surface chemistry and performance of graphite negative electrodes for Li ion batteries, Electrochimica Acta 45 (1999) 67–86, http://dx.doi.org/10.1016/S0013-4686(99)00194-2.
[85] M.J. van Setten, V.A. Popa, G.A. de Wijs, G. Brocks, Electronic structure and optical properties of lightweight metal hydrides, Phys. Rev. B 75 (2007) 035204, http://dx.doi.org/10.1103/PhysRevB.75.035204.
[86] S.S. Zhang, K. Xu, T.R. Jow, EIS study on the formation of solid electrolyte interface in Li-ion battery, Electrochimica Acta 51 (2006) 1636–1640, http://dx.doi.org/10.1016/j.electacta.2005.02.137.
[87] M. Schäfer, K.-M. Weitzel, Bombardment induced ion transport. Part I: numerical investigation of bombardment induced ion transport through glasses and membranes on the basis of the Nernst–Planck–Poisson equations, Phys. Chem. Chem. Phys. 13 (2011) 20112, http://dx.doi.org/10.1039/c1cp21215j.
[88] K. Tasaki, A. Goldberg, J.-J. Lian, M. Walker, A. Timmons, S.J. Harris, Solubility of lithium salts formed on the lithium-ion battery negative electrode surface in organic solvents, J. Electrochem. Soc. 156 (2009) A1019, http://dx.doi.org/10.1149/1.3239850.